Applied Catalysis B: Environmental 179 (2015) 171–177

Contents lists available at ScienceDirect

Applied Catalysis B: Environmental

journal homepage: www.elsevier.com/locate/apcatb

Tetrachlorobiphenyl removal from sludge matrix using mixed crystal $Ti_{0.97}Fe_{0.02}Ni_{0.01}O_2$ thin film

Tolga Tunçal[a,*], Deniz İzlen ÇİFÇİ[a], Orhan USLU[b]

[a] Namık Kemal University, Çorlu Engineering Faculty, Environmental Engineering Department, 59860 Çorlu, Tekirdağ, Turkey
[b] Yeditepe University, Engineering Faculty, Civil Engineering Department, 26 Ağustos Kampüsü, Kayışdağı Caddesi, 34755 Ataşehir, İstanbul, Turkey

ARTICLE INFO

Article history:
Received 18 March 2015
Received in revised form 3 May 2015
Accepted 6 May 2015
Available online 7 May 2015

Keywords:
Tetrachlorobiphenyl
Industrial sludge
Thin film
Photocatalytic treatment
Chlorination
PCBs

ABSTRACT

In this study, 2,2′,5,5′-tetrachlorobiphenyl removal from activated sludge matrix using thin film (TF)-based photocatalytic (PCT – TF + UVC + H_2O_2) and UVC + H_2O_2 (photolytic) treatment systems were investigated for three different initial sludge pH_i values of 3.0 ± 0.1; 7.3 ± 0.1 and 10.0 ± 0.1. A novel, visible light active Ti:Fe:Ni nano composite TF was successfully synthesized and used as catalyst. The fabricated TF was characterized by SEM, TEM, XRD, XPS and UV–vis spectroscopy methods. Experimental results indicated that while raw industrial sludge contains only 2,2′,5,5′′-tetrachlorobiphenyl, treated sludge samples contained more chlorinated PCB congeners in descending chlorination order from 2,2′,3,3′,4,4′,5,5′,6,6′ decachlorobiphenyl to 2,3′,4,4′,5 pentachlorobiphenyl. Experimental results also indicated that 2,2′,5,5′-tetrachlorobiphenyl was removed from the sludge matrix by only TF-based PCT that was carried out at neutral pH_i. In addition, UVC + H_2O_2 system caused significant PCB formation at all studied pH levels. PCB generation/degradation reactions followed pseudo-first order reaction kinetics. Obtained results also proposed that UV irradiation can induce C—Cl bond cleavage in chlorinated compounds yielding •Cl radicals, responsible for further chlorination. The k_{obs} value observed in 2,2′,5,5′-tetrachlorobiphenyl degradation by TF-based PCT at $pH_i = 7.3 \pm 0.1$ was 0.0169 ± 10^{-3} min^{-1} and 1.5 times higher than at $pH_i = 3.0 \pm 0.1$. The observed k_{obs} values in TF based PCT for PCB generation at $pH_i = 3.0 \pm 0.1$ and $pH_i = 10.0 \pm 0.1$ were 0.0037 ± 10^{-3} and 0.0015 ± 10^{-3} min^{-1}, respectively.

1. Introduction

As a result of rapid industrialization, more and more industrial sludge has been generated during wastewater treatment. One of the related significant problems is generation of industrial sludge that contains various organic or inorganic hazardous compounds. Polychlorinated biphenyls (PCBs) are amongst the most abundant organic contaminants present in sludge. These compounds have been widely used as heat-transfer and hydraulic fluids, solvent extenders, plasticizers, flame retardants, and dielectric fluids since they have thermal and chemical stability [1,2].

Due to their persistence and potential impact on humans and wildlife, PCBs were listed in the Stockholm Convention on Persistent Organic Pollutants (POPs) to prevent further environmental contamination [3]. Sandal [4] et al., (2008) studied effects of two structurally different congeners of the same molecular weight, ortho-substituted, non-coplanar congener, 2,2,5,5′-tetrachlorobiphenyl, and a non-ortho-substituted coplanar congener with dioxin-like activity, 3,3′,4,4′-tetrachlorobiphenyl on cultured human peripheral lymphocytes. They concluded that both the non-coplanar and the coplanar PCB cause DNA damage, and that the ortho-substituted congener (2,2,5,5′-tetrachlorobiphenyl) was significantly more potent than the dioxin-like coplanar congener.

Several treatment methods including aerobic biodegradation [5–8], Fenton's reagent [9–12], L-lysines/PAA/PVDF membrane process [13] and heterogenic photocatalysis [14–16] have been investigated for the removal of PCB congeners from various contaminated mediums. However, these methods have drawbacks that limit their full-scale applications. In heterogenic photocatalysis nano-TiO_2 powder is added to the reaction mixture. Remaining nano-scale catalyst at the end of the treatment period also poses serious environmental health risks and thus requires advanced sep-

Abbreviations: DS, dry solids; MLSS, mixed liquor suspended solids; MLVSS, mixed liquor volatile suspended solids; PCB(s), polychlorinated biphenyls; POPs, persistent organic pollutants; pH, $_i$initial pH value; PCT, photocatalytic treatment; SEM, scanning electron microscopy; TEM, transmission electron microscopy; TOC, total organic carbon; TF, thin film; TQR, tubular quartz reactor; VS, volatile solids; XPS, X-ray photoelectron spectroscopy; XRD, X-ray diffraction.

* Corresponding author. Tel.: +90 282 250 23 44; fax: +90 282 250 99 24.
E-mail address: ttuncal@nku.edu.tr (T. Tunçal).

http://dx.doi.org/10.1016/j.apcatb.2015.05.011
0926-3373/

aration processes. Pure or doped TiO_2 thin films (TFs) grown on different materials require no further separation and thus attracted much attention in recent years [17]. Although Ti:Ni and Ti:Fe nanocomposites have been well-investigated, photocatalytic activity of a nanomaterial composed of triple combination of these elements has not been investigated yet. Moreover, decreasing recombination rate by Ni^{+2} ions and generation of photo-Fenton reactions by Fe^{+2}/Fe^{+3} in addition to Ti^{+4}/Ti^{+3} based photocatalytic reactions through the same nano-composite-TF could provide significant benefits for photocatalytic environmental pollution control.

Although PBCs are one of the most abandoned POPs in sludge, there are very limited studies explaining their degradation or formation mechanisms. In addition, most of the surveyed literature on PCB removal through several advanced oxidation processes indicated strong acidic pH values as being preferred [12,16]. Although these studies have investigated PCB degradation pathways through identifying generated intermediates, formation of new PCB compounds and the mechanism behind the further chlorination has not been explained yet. Moreover, identification and fate of chlorinated organic compounds in UV based treatment systems have also attracted significant attention. There is also limited understanding of the potential effect of combined UV/chlorine conditions on the formation of regulated or emerging pollutants [18].

In this study, 2,2′,5,5′-tetrachlorobiphenyl removal from activated sludge matrix using TF–based PCT and UVC + H_2O_2 treatment systems were investigated systematically for the variable pH_i levels. The fabricated TF(s) were characterized by SEM, TEM, XRD, XPS and UV–vis spectroscopy. The PCT was carried out using a tubular quartz reactor (TQR) of which inner surface was coated by Ti:Fe:Ni TF. PCB congeners present in raw and treated sludge samples were identified using GC–MS and TOC measurements in order to investigate the impacts of the applied treatment methods and experimental conditions.

2. Material and methods

2.1. Sol–gel preparation

Fe: Ni-doped TiO_2 TFs were prepared using the sol–gel dip-coating technique. The TiO_2 sol was prepared using Titanium(IV) isopropoxide (TTIP) 97% (Fluka) as Ti precursor, $Fe(NO_3)_3 9H_2O$ and $NiCl_2 6H_2O$ (Merck) as source of Fe and Ni elements and ethanol as solvent. TTIP was slowly added to the pre-acidified ethanol with stirring under nitrogen atmosphere [19]. A secondary solution was prepared mixing glacial acetic acid with deionized water in order to decrease the kinetics of the hydrolysis and polycondensation. This secondary solution was mixed for one hour and gradually added dropwise to the TTIP solution. Fe:Ni sol was prepared by dissolving $Fe(NO_3)_3 9H_2O$ and $NiCl_2 6H_2O$ (Merck) in diluted HNO_3 and ethanol solutions. The optimum Ti:Fe:Ni atomic ratio was determined to be 0.97:0.02:0.01 (wt%). After being vigorously stirred for an hour, stable and homogenous Ti and Fe:Ni sols were obtained. The obtained sol–gels were stirred under UVC irradiation for an hour before dip-coating. The sol–gel temperature was maintained at room temperature 25 °C during dip coating to control the film thickness.

2.2. Thin film coating procedures and photoreactor configuration

The photocatalytic experiments were performed with TQR(s) and carried out in Luzchem UV Photoreactor equipped with sixteen light lamps (UV-C Osram) at 25 °C. The dimensions of the TQR were 150 × 30 mm in length and diameter, respectively. Only inner surface of TQR was coated by TF(s) to increase light transmittance. TF(s) were grown by multiple layer dip-coating on TQR. To create a p-n junction, inner surface of TQR was firstly coated with a Ti layer and Fe: Ni layer was then coated on to the surface as a second layer. The as-prepared wet films were dried at 300 °C for 10 min. Finally, the films were annealed at 500 °C for 1 h. A KSV Nima Medium Dip Coater Unit was used for TF fabrication. The photoreactor equipped with sixteen fluorescent UVC lamps (8 Watt) provided an illuminated area of approximately 0.092 m^2, which had an active area of approximately 0.061 m^2 that experienced fluctuations of less than 8% in the incident power. The UVC power intensity was measured with a power meter supplied by Luzchem. The measured average UVC energy was 1057 ± 15 joules. Uncoated outer surface of the TQR was carefully cleaned with acetone and deionized water prior to each photocatalytic experiments to improve light penetration. The TQR with 100 ml industrial sludge was placed vertically into the photoreactor and exposed to the above described irradiation conditions. The uncoated TQR was also used as a control to determine the photolytic (with and without H_2O_2 addition) PCB degradation rates. The H_2O_2 dosage ratios for both photocatalytic and photolytic experiments were held constant at 0.02 g H_2O_2 g^{-1} VSS.

Table 1
Physicochemical properties of the industrial sludge.

Parameter	Unit	Value
pH	–	7.3 ± 0.1
Cond.	$\mu s\,cm^{-1}$	3.2 ± 1.8
MLSS	$g\,L^{-1}$	5.8 ± 2.1
MLVSS	$g\,L^{-1}$	4.3 ± 1.5
DS	%	0.6 ± 0.1
TOC	$g\,kg^{-1}$	60 ± 5

2.3. Structural characterization

The appearance and structure of TF surfaces were studied by SEM that was performed using a JEOL JSM 6060. Prior to SEM analysis, the samples were coated with gold to increase the conductivity. Electron micrographs from the surface were taken utilizing a low voltage (5 kV) charge balance. The microscopic structure of the films was characterized by high-resolution transmission electron microscopy (JEOL JEM 2100F TEM). The crystallinity, crystallite size and phase relationship of the TiO_2 TF(s) were characterized by XRD analysis. The diffraction data was collected with a Rigaku D/MAX-2200/PC diffractometer utilizing Bragg–Brentano geometry and a Cu-Kα radiation source with a monochromator in front of the X-ray detector. XPS measurements were performed on a Thermo Scientific K-ALPHA operating at 12.0 kV and 3 mA. Ultraviolet–visible (UV–vis) absorbance spectra was obtained using a SHIMADZU UV-1800 instrument.

2.4. Sample preparation and chemical analysis procedures

Activated sludge samples were collected from aeration tank of an industrial wastewater treatment plant. Freshly collected samples were placed in clean glass jars. Both the raw and the treated samples were maintained in a refrigerator at +4 °C for PCB analysis. Collection and analysis of samples were performed according to previous published protocols [20]. The sludge moisture content was determined using Presica XM 60 Moisture Analyzer. TOC was determined by High-Temperature Combustion/(SM 5310) method. Samples were heated in an oven at 600 °C for 90 min and then were cooled to 25 °C. The total organic carbon (TOC) analysis was carried out using Hach-Lange® IL-550 TOC analyzer. Typical sludge characteristics are summarized in Table 1. All measurements were duplicated.

The microwave extraction method (EPA Method 3546) was used to extract PCB compounds from the sludge matrix. All of the samples were extracted using a 1:1 hexane:acetone mixture solution.

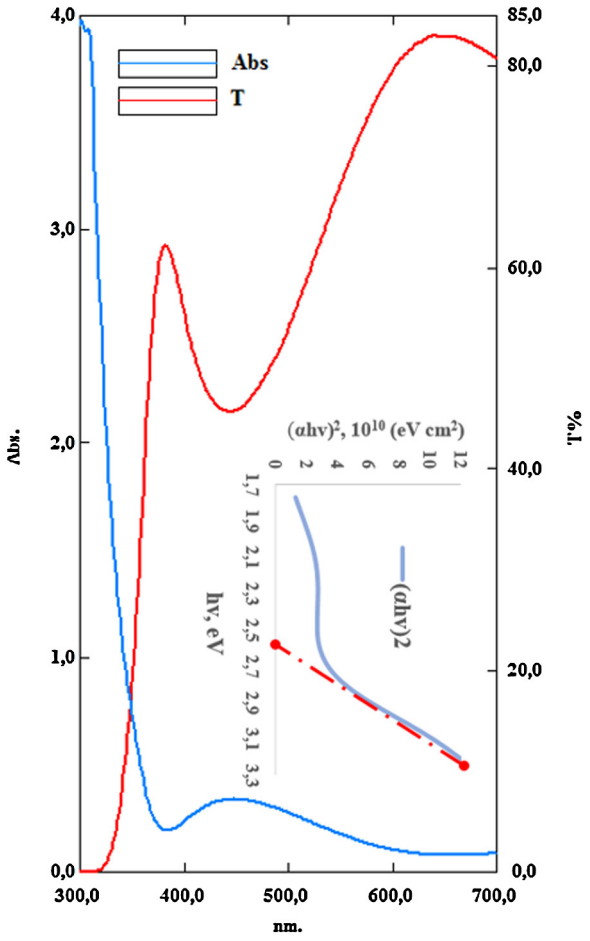

Fig. 1. UV–vis spectrum and in set of the optical energy gap for Ti:Fe:Ni TF.

The content of sludge organic matter (VSS) was determined by loss of ignition in a muffle furnace at 550 °C for 3 h using Standard Method 2540-E [21]. All of the extracts were analyzed for 15 PCB congeners with an Agilent 7890A gas chromatograph (GC) equipped with an electron capture detector (ECD). EPA method 8082 A was employed to perform the PCB analyses. Agilent DB-XLB (30 m, 0.25 mm, 0.25 mm) column was used for PCB chromatography. The initial oven temperature was maintained at 70 °C for 2 min and then raised to 150 °C at 25 °C min^{-1}, to 200 °C at 3 °C min^{-1}, and to 280 °C at 8 °C min^{-1}, and this temperature was maintained for 10 min. The injector, ion source, and quadrupole temperatures were adjusted to 250 °C, 230 °C, and 150 °C, respectively. High purity helium was used as the carrier gas in constant flow mode (1.5 ml min^{-1}, 45 cm s^{-1} linear velocity). The compounds were identified based on their retention times. Target and qualifier ions were quantified using the internal standard calibration procedure [20].

3. Results and discussion

3.1. Structural characterization results

Fig. 1 shows the UV–vis absorption and transmittance spectrum of the TF coated on quartz substrate. The TF are highly transparent up to 80% in the visible region with a broad absorption edge between 400 nm and 500 nm. Individual peaks of Ti, Fe and Ni elements are not apparent in the UV–vis spectra, indicating newly formed energy levels in the fabricated nano-composite. The high transmittance indicates smooth TF surface and relatively good film homogeneity. The absorption edge shifts remarkably towards the higher wavelength side than pure TiO_2 indicating reduced band gap energy that can be calculated using Eq. (1).

$$\alpha = \frac{\alpha_0 \left(h\nu - E_g\right)^n}{h\nu} \quad (1)$$

The band gap energy (E_g) is determined by extrapolating straight line portion of $(\alpha h\nu)^2$ vs $h\nu$ spectrum to $\alpha = 0$. Where α and hν are absorption coefficients of the film and the incident photon energy respectively. The optical energy gap for $Ti_{0.97}Fe_{0.02}Ni_{0.01}O_2$ film is shown in inset of Fig. 1. A direct band gap of 2.56 eV was determined for as-deposited TF. The absorption in the visible region is enhanced significantly in $Ti_{0.97}Fe_{0.02}Ni_{0.01}O_2$ TF. This indicates the TF has smaller band gap energy than that of pure TiO_2 (3.20 eV). The significant red-shift with lower band energy may be due to the difference in the surface states [22].

The SEM image of the TF in Fig. 2(a) exhibits porous structure, where Fe_2O_3, NiO and TiO_2 nanoparticles are randomly scattered across the entire layer, forming pore and gaps on the film. The SEM image suggests that the TF has uniform grain distribution with well-connected grains. Fig. 2b shows the TEM image of the TF. The grains are slightly aggregated due to high surface energy associated with the particles during the film growth [23]. The dark patches seen in Fig. 2(b) indicated the regions which show the incorporation of Fe_2O_3 and NiO into the TiO_2 matrix [24,25].

XPS spectrum indicated that the film deposited on quartz contains Ti, O, Fe and Ni elements. The atomic percentages of Ti, O, Fe, and Ni on the surface of the film were 28.67, 68.26, 2.31 and 0.76%, respectively. As a rechecking for the stoichiometric formation of TiO_2, the O/Ti ratio was determined to be 2.4, which exhibits excess oxygen content related to hydroxyl groups and film density [26]. Fig. 3(a) shows the high resolution XPS spectrum of the Ti 2p core level. The peaks were observed at the binding energies (BE) of 458.7 eV for 2p3/2 and 464.4 eV for 2p1/2, corresponding to 5.7 eV spin–orbit coupling of Ti(IV) chemical state [27,28]. Two other small peaks at 457.6 eV and 463.5 eV were related to the presence of a small amount of Ti^{3+} chemical state. Fig. 3 (b) shows the high resolution XPS spectrum of the O 1s core level. The peaks observed at 530.5 and 531.4 eV could correspond to Ti-O-Fe in TiO_2 and the hydroxyl group, respectively.

As can been seen in Fig 3(c) The doublet lines of Fe corresponding to 2p3/2 and 2p1/2 were observed at 723.8 eV and 712.6 eV, respectively which is due to spin–orbit splitting. For Fe 2p3/2 level, the BE values depend on the oxidation state of the iron: (i) in metallic iron state (Fe 0), the BE of Fe 2p3/2 is in the range of 706.7–707.4 eV, (ii) in the Fe^{2+} state, the range is 709.3–710.0 eV, and (iii) in the Fe^{3+} state, the range is between 710.6 and 711.6 eV [29,30]. Presence of satellite peak at BE of 715–716 eV confirms FeO formation and presence of Fe_2O_3 at 719.0–719.8 eV [31,32]. The XPS studies indicated the presence of Fe^{3+} and oxygen in O^{2-} chemical states; confirming the formation of Fe_2O_3. The shoulder of the Ti (2p3/2) peak corresponds to a band at 459.1 eV. This band is assigned to formation of a Ti—O—Fe bond in the interface of the thin film. Fig. 3(d) depicts the Ni 2p core level XPS spectra of the TF. It was found that the binding energy of Ni 2p3/2 is at 856.18 eV. This is different from those of metal Ni^0 (852.6 eV) and Ni^{3+} (856.1 eV) [33], and very near that of Ni^{2+} (855 eV) [34,35], which implies that the main chemical valence of Ni in the film is in +2.

3.2. Tetrachlorobiphenyl removal from sludge matrix by photocatalysis at different initial pH values

Photolytic and photocatalytic decomposition of 2,2′,5,5′-tetrachlorobiphenyl was observed under acidic, basic and neutral conditions. Fig. 4 shows GC–MS spectrums of raw and treated

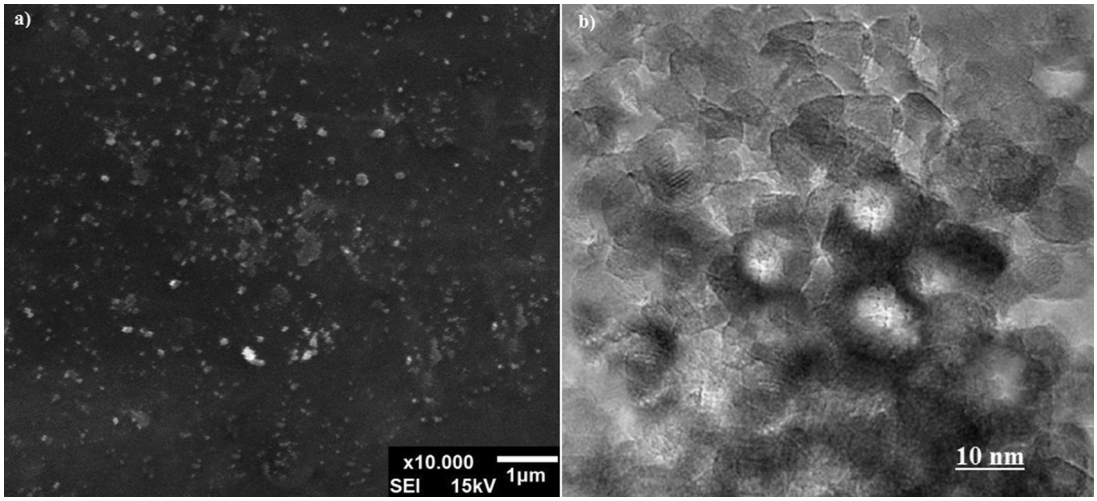

Fig. 2. SEM and TEM images of the TF.

industrial sludge samples. While the raw sludge contains only 2,2′,5,5′-tetrachlorobiphenyl, treated samples included more chlorinated PCBs except for TF-based PCT conducted at $pH_i = 7.3 \pm 0.1$. The figure clearly indicates that chlorination reactions occur during both photolysis and TF-based PCT, resulting with formation of new PCB species that start with the least chlorinated 2,2′,5,5′-tetrachlorobiphenyl to ultimate chlorinated 2,2′,3,3′,4,4′,5,5′,6,6′-decachlorobiphenyl. As can be seen from the Fig. 4, TF-based PCT removed 2,2′,5,5′-tetrachlorobiphenyl from sludge matrix successfully around neutral/slightly acidic pH values without generating new PCBs. Experimental results also proposed that relatively higher numbers of PCB congeners were detected under strong alkaline conditions without any removal taking place. This result could be ascribed to both inhibited PCB adsorption onto the TF surface as a result of repulsive forces and inhibited $OH^{\bullet}$ radical production through photolytic/photocatalytic H_2O_2 decomposition. Although, TF-based PCT carried out in strong acidic conditions produced several chlorinated PCB compounds in initial 4 h, the amounts of these PCBs eventually decreased from 2.41 ± 0.1 mg kg^{-1} to 0.342 ± 0.1 mg kg^{-1} in the following 2-hours. However similar reactions were not observed in H_2O_2 + UV-C (photolytic) treatment period, which resulted in significant PCB formation without any subsequent degradation. This result reveals that $Ti_{0.97}Fe_{0.02}Ni_{0.01}O_2$ TF provided significant contribution to PCB removal from sludge matrix. Time dependent mass fractional PCB distributions observed under different experimental conditions were also depicted in Fig. 5. Experiments conducted at strong acidic conditions resulted with hydrogen abstraction and chlorine bounding to 2,2′,5,5′-tetrachlorobiphenyl instead of hydroxylation reactions. Obtained results also proposed that PCB formation occurs

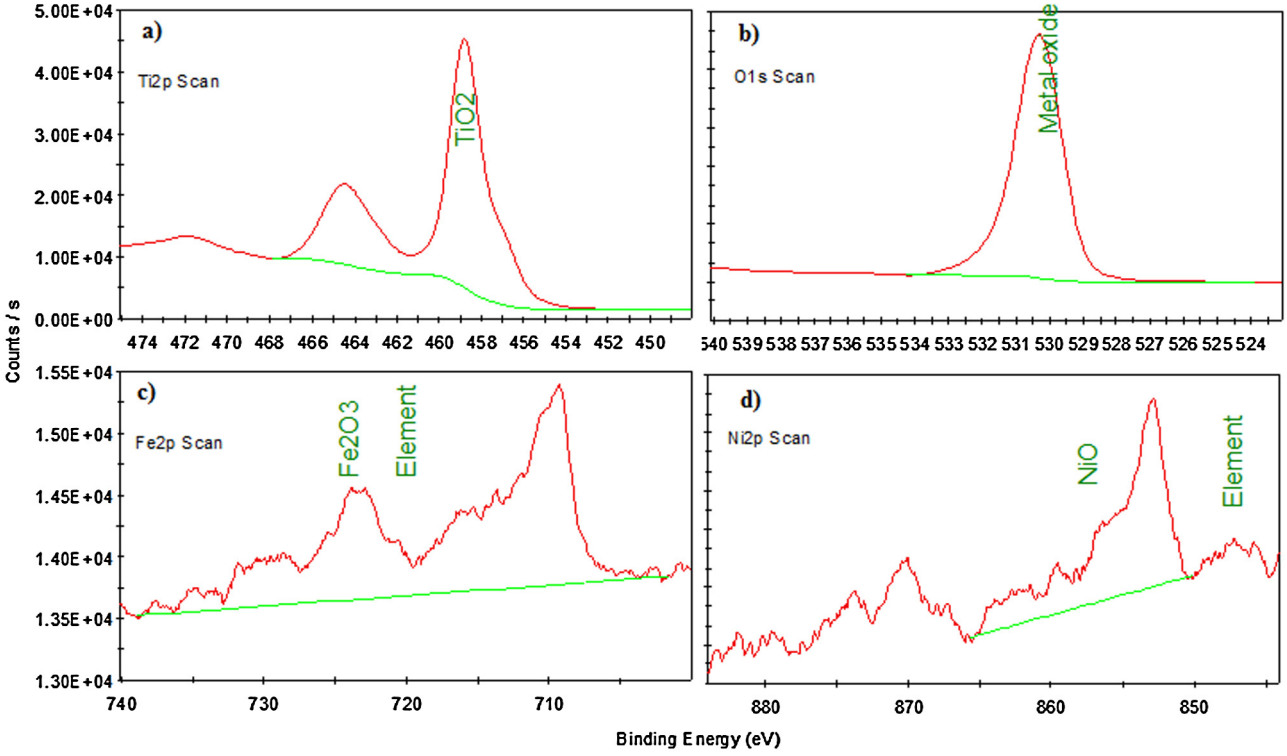

Fig. 3. The XPS spectra of Fe:Ni doped TiO_2 TF (a) Ti 2p, (b) O 1s, (c) Fe 2P, (d) Ni 2P scans.

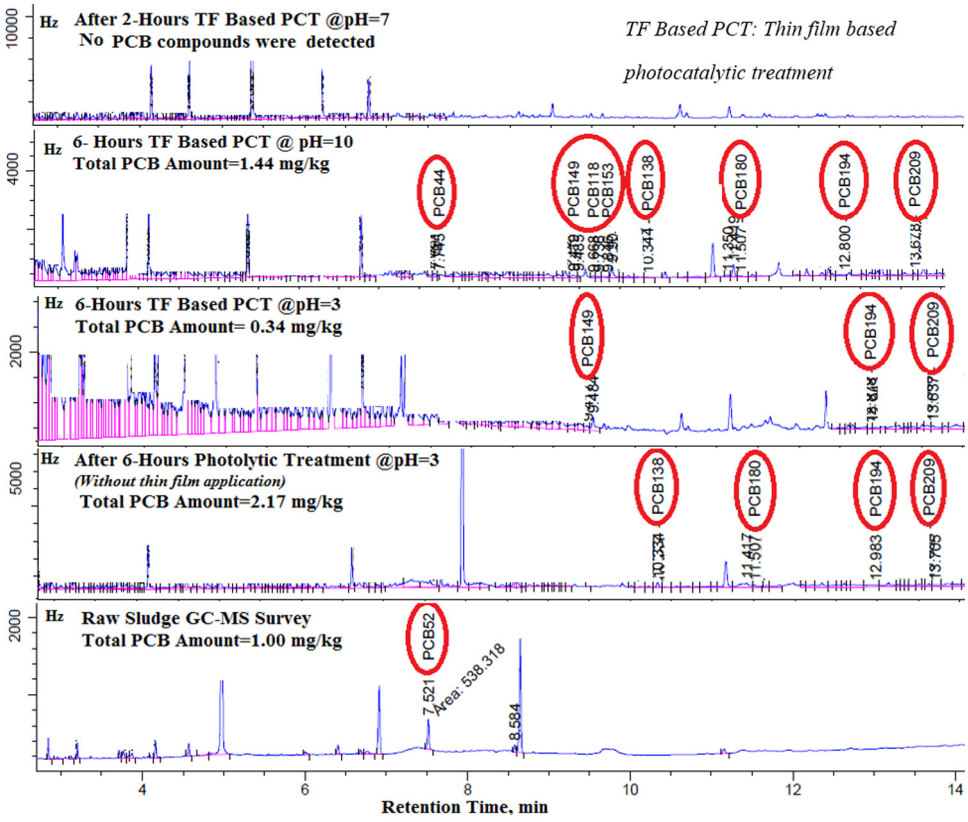

Fig. 4. GC–MS spectrums of raw and treated industrial sludge samples.

as sequential reactions in bulk sludge matrix. However mineralization of 2,2′,5,5′-tetrachlorobiphenyl occurs only in TF-based PCT between nanoparticle-sludge interface. Therefore photo-induced holes (h^+) and surface hydroxyl groups formed/present on the TF played an important role in PCB oxidation.

Sludge organic matter is mainly composed of proteins present in endogenic polymeric substances (EPS). The functional RCOOH and $RCOO^-$ groups present in proteins contribute to the overall surface charge [36]. Electron transfer between TiO_2 TF surface and proteins with different isoelectric points have been investigated through a TiO_2 TF system [37]. In this study, an electrochemical method was used to determine pKa of the TiO_2 TF and it was measured to be 6.27. Furthermore a direct electron transfer between proteins and nanostructured TiO_2 TF surfaces at pH 7.0 has been observed and the proteins have been verified to be stably immobilized onto the TiO_2 TF. This result is in well agreement with direct PCB miner-

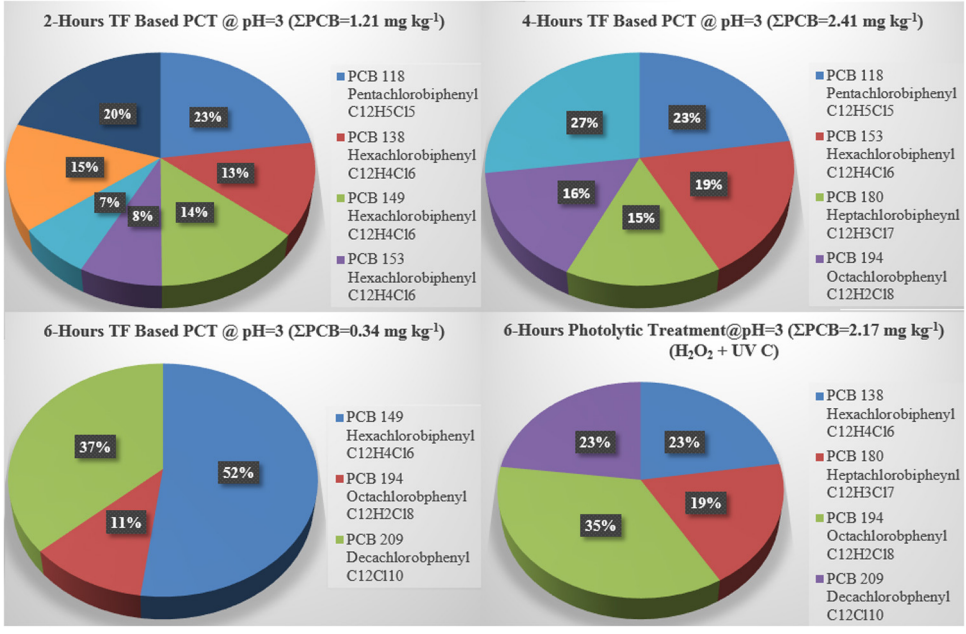

Fig. 5. Percentage distribution and the concentrations of detected PCBs for variable treatment conditions.

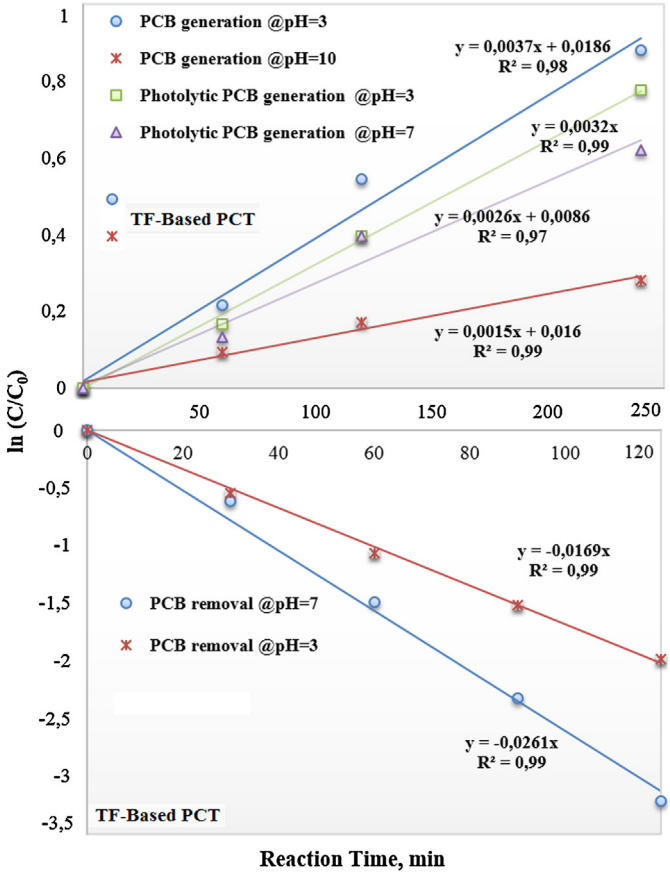

Fig. 6. Effect of the initial pH on the decomposition and formation rates of ΣPCB_{15}.

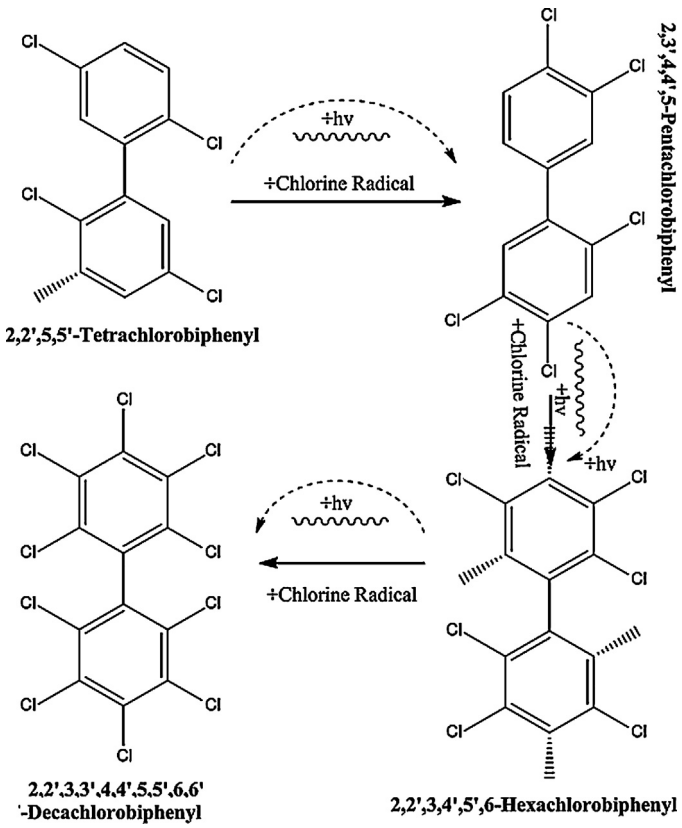

Fig. 7. Graphical model explaining the further chlorination of 2,2′,5,5′-tetrachlorobiphenyl by UV-C irradiation.

alization, by photo-induced holes (h^+) at neutral pH observed in this study. Acknowledging the result, phase transition of 2,2′,5,5′-tetrachlorobiphenyl from wastewater to sludge interface could also be explained with adsorption onto EPS structure rather than microbial PCB degradation theory.

The decomposition and in-situ generation of PCB congeners followed pseudo-first order kinetics. Fitting results of the pseudo-first-order model to the rate data of PCB decomposition/generation under various pH levels are presented in Fig. 6 (a), (b). The k_{obs} value observed in 2,2′,5,5′-tetrachlorobiphenyl degradation through TF-based PCT at neutral pH was 0.0169 ± 10^{-3} min^{-1} and was 1.5 times higher than the measured value at the acidic conditions. It should be also taken into consideration that no PCB degradation was observed at the first 4 h of PCT at $pH_i = 3.0 \pm 0.1$. It can be safely concluded that PCB degradation rate is higher at neutral pH. The observed k_{obs} values in TF based PCT for PCB generation at $pH_i = 3.0 \pm 0.1$ and $pH_i = 10.0 \pm 0.1$ were 0.0037 ± 10^{-3} and 0.0015 ± 10^{-3} min^{-1}, respectively. Obtained results also proposed that UV irradiation can induce C—Cl bond cleavage in chlorinated compounds yielding •Cl radicals. Several studies have also reported that UV irradiation can cause C—Cl bond dissociation [38,39]. As can be seen in the Fig. 6 (a), $C\,C_0^{-1}$ ratios are higher than one as a result of formation of new PCB species. In situ generated chloride radicals could be originated from photolytic disassociation reactions that occur in chlorinated organic molecules present in the sludge matrix.

Although higher numbers of PCB congeners were detected at alkaline pH level, slower first-order PCB generation kinetics were observed as compared to the acidic pH levels. The observed k_{obs} values in H_2O_2 + UVC system for PCBs generation at $pH_i = 3.0 \pm 0.1$ and $pH_i = 7.3 \pm 0.1$ were 0.0032 ± 10^{-3} min^{-1} and 0.0026 ± 10^{-3} min^{-1}. These values are very close to the k_{obs} obtained from TF-based PCT at $pH_i = 3.0 \pm 0.1$. Consequently PCB generation could be ascribed to photolysis. By the effect of UVC irradiation, the disassociated chloride ions are converted to chloride radicals as described in Eq. (1). Hydroxyl and chlorine radicals are strong electrophilic species and can attack electron-rich aromatic rings by H^+-abstraction and electron transfer. Since the concentration of hydroxyl ions are very low at acidic pH levels, chloride radicals are directly bounded to organic molecules instead of hydroxyl groups. PCB generation at strong alkaline condition could also be attributed to hydroxyl tension, promoting hydrogen removal and chlorination as described in reaction 2. A model explaining the further chlorination in sludge matrix under UVC irradiation was also schematized in Fig. 7.

$$Cl^- \xrightarrow{\lambda<260nm} Cl^\bullet + e^- \quad (1)$$

$$R - H + Cl^\bullet \xrightarrow{chlorination} R - Cl + H^+ \quad (2)$$

4. Conclusions

In this study, 2,2′,5,5′-tetrachlorobiphenyl removal from sludge using $Ti_{0.97}Fe_{0.02}Ni_{0.01}O_2$ TF and photolytic treatment systems were investigated under acidic, neutral and basic pH levels. The most important result obtained from the present study is that TF-based PCT application around neutral/slightly acidic pH is vital to control the PCB congeners present in sludge. Obtained results also implied that UVC irradiation leads to formation of chlorine radicals and subsequent chlorination reactions in bulk sludge interface. Therefore, UVC based treatment systems, employed in both water and wastewater treatment, especially when applied within the presence of free chlorine or chlorinated organic compounds could trigger formation of highly toxic compounds. Since UVC irradiation could pose more serious environmental risks, effluents of full-scale water or wastewater treatment plants employing low-

pressure lamps (λmax≈254 nm) should be monitored for PCBs or other halogenated compounds. Experimental results also indicated that in situ generated PCB congeners with six chlorine atoms like 2,2′,3,4′,5′,6 hexachlorobiphenyl, 2,2′,3,3′,4,4′,5,5′ octachlorobiphenyl and 2,2′,3,3′,4,4′,5,5′,6,6′ decachlorobiphenyl are more recalcitrant to photo-degradation as compared to the less chlorinated PCBs.

Acknowledgments

This work is funded by The Scientific and Technological Research Council of Turkey TÜBİTAK (Project 111Y209) and Çerkezköy Organized Industrial Zone Management.

Appendix A. Supplementary data

Supplementary data associated with this article can be found, in the online version, at http://dx.doi.org/10.1016/j.apcatb.2015.05.011

References

[1] D.A. Abramowicz, M.J. Brennan, H.M. Van Dort, E.L. Gallagher, Environ. Sci. Technol. 27 (6) (1993) 1125–1131.
[2] T. Tunçal, O. Uslu, J. Environ. Manage. 149 (2015) 37–45.
[3] B.O. Clarke, N.A. Porter, P.J. Marriott, J.R. Blackbeard, Environ. Int. 36 (4) (2010) 323–329.
[4] S. Sandal, B. Yilmaz, D.O. Carpenter, Mutat. Res. -Gen. Tox. En. 654 (1) (2008) 88–92.
[5] R. Unterman, M.J. Brennan, R.E. Brokks, C. Johnson, Biotechnology for Degradation of Toxic Chemicals in Hazardous Wastes, in: R.J.E.D. Scholze Smith Jr., J.T. Bandy, Y.C. Wu, J.V. Basilico (Eds.), Noyes Data Corporation, New Jersey, 1988, p. 376.
[6] V.H. Pellizari, S. Bezborodnikov, J.F. Quensen, J.M. Tiedje, Appl. Environ. Microbiol. 62 (1996) 2053–2058.
[7] Y.C. Chang, K. Takada, D. Choi, T. Toyama, K. Sawada, S. Kikuchi, Appl. Biochem. Biotechnol. 170 (2013) 381–398.
[8] M. Song, C. Luo, F. Li, L. Jiang, Y. Wang, D. Zhang, G. Zhang, Sci. Total Environ. 502 (2015) 426–433.
[9] K. Dercová, B. Vrana, R. Tandlich, Chemosphere 39 (15) (1999) 2621–2628.
[10] J.J. Pignatello, E. Oliveros, A. MacKay, Crit. Rev. Environ. Sci. Technol. 36 (1) (2006) 1–84.
[11] E.G. Garrido-Ramirez, B.K.G. Theng, M.L. Mora, Appl. Clay Sci. 47 (2010) 182–192.
[12] Z.R. Lin, X.H. Ma, L. Zhao, Y.H. Dong, Chemosphere 101 (2014) 15–20.
[13] B. Seteni, J.C. Ngila, K. Sikhwivhilu, R.M. Moutloali, B. Mamba, Phys. Chem. Earth Pt A/B/C 66 (2013) 60–67.
[14] P.C. Zhang, R.J. Scrudato, J.J. Pagano, R.N. Roberts, Chemosphere 26 (6) (1993) 1213–1223.
[15] Q. Huang, C.S. Hong, Chemosphere 41 (6) (2000) 871–879.
[16] K.H. Wong, S. Tao, R. Dawson, P.K. Wong, J. Hazard. Mater. 109 (1) (2004) 149–155.
[17] P.J. Lu, C.W. Chien, T.S. Chen, J.M. Chern, Chem. Eng. J. 163 (1) (2010) 28–34.
[18] L. Deng, C.H. Huang, Y.L. Wang, Environ. Sci. Technol. 48 (5) (2014) 2697–2705.
[19] Y.C. Lin, H.S. Lee, J. Hazard. Mater. 179 (1) (2010) 462–470.
[20] A. Sofuoğlu, M. Odabaşı, Y. Taşdemir, N.R. Khalili, T.M. Holsen, Atmos. Environ. 35 (2001) 6503–6510.
[21] APHA-AWWA-WPCF, Standard Methods for the Examination of Water and Wastewater, 20th ed., American Public Health Association, Washington, DC, 1998.
[22] R.T. Sapkal, S.S. Shinde, T.R. Waghmode, S.P. Govindwar, K.Y. Rajpure, C.H. Bhosale, J. Photochem. Photobiol. B: Biol. 110 (2012) 15–21.
[23] Y. Wang, Y. Hao, H. Cheng, J. Ma, B. Xu, W. Li, S. Cai, J. Mater. Sci. 34 (12) (1999) 2773–2779.
[24] Y. Von Lim, H. Fan, Z. Shen, C.H. Kang, Y. Feng, S. Wang, Appl. Phys. A 95 (2) (2009) 555–562.
[25] G. Yang, Z. Yan, T. Xiao, Appl. Surf. Sci. 258 (22) (2012) 8704–8712.
[26] Z. Wang, U. Helmersson, P.O. Käll, Thin Solid Films 405 (1) (2002) 50–54.
[27] J. Yu, X. Zhao, Q. Zhao, Mater. Chem. Phys. 69 (1) (2001) 25–29.
[28] O. Akhavan, E. Ghaderi, K. Rahimi, J. Mater. Chem. 22 (43) (2012) 23260–23266.
[29] O. Akhavan, Appl. Surf. Sci. 257 (2010) 1724–1728.
[30] X. Zhang, L. Lei, Appl. Surf. Sci. 254 (2008) 2406–2412.
[31] M. Saleem, M.F. Al-Kuhaili, S.M.A. Durrani, I.A. Bakhtiari, Phys. Scr. 85 (5) (2012) 55802.
[32] M.A. Mahadik, S.S. Shinde, V.S. Mohite, S.S. Kumbhar, A.V. Moholkar, K.Y. Rajpure, V. Ganesan, J. Nayak, S.R. Barman, C.H. Bhosale, J. Photochem. Photobiol. B: Biol. 133 (2014) 90–98.
[33] A.P. Grosvenor, M.C. Biesinger, R.S.C. Smart, N.S. McIntyre, Surf. Sci. 600 (9) (2006) 1771–1779.
[34] S.Y. Han, D.H. Lee, Y.J. Chang, S.O. Ryu, T.J. Lee, C.H. Chang, J. Electrochem. Soc. 153 (6) (2006) C382–C386.
[35] N. Bahadur, R. Pasricha, S. Chand, R.K. Kotnala, Mater. Chem. Phys. 133 (1) (2012) 471–479.
[36] G. Chen, K.A. Strevett, Environ. Microbiol. 3 (4) (2001) 237–245.
[37] Y. Luo, Y. Tian, A. Zhu, H. Liu, J. Zhou, J. Electroanal. Chem. 642 (2) (2010) 109–114.
[38] H. Morrison, K. Muthuramu, D. Severance, J. Org. Chem. 51 (24) (1986) 4681–4687.
[39] J. Li, E.R. Blatchley, Environ. Sci. Technol. 43 (1) (2008) 60–65.